Measurement of the ^{13}C isotopic signature of methane emissions from northern European wetlands

Rebecca E. Fisher[1], James L. France[1,2], David Lowry[1], Mathias Lanoisellé[1], Rebecca Brownlow[1], John A. Pyle[3,4], Michelle Cain[3], Nicola Warwick[3,4], Ute M. Skiba[5], Julia Drewer[5], Kerry J. Dinsmore[5], Sarah R. Leeson[5], Stéphane J.-B. Bauguitte[6], Axel Wellpott[6], Sebastian J. O'Shea[7], Grant Allen[7], Martin W. Gallagher[7], Joseph Pitt[7], Carl J. Percival[7], Keith Bower[7], Charles George[8], Garry D. Hayman[8], Tuula Aalto[9], Annalea Lohila[9], Mika Aurela[9], Tuomas Laurila[9], Patrick M. Crill[10], Carmody K. McCalley[11], and Euan G. Nisbet[1]

[1]Department of Earth Sciences, Royal Holloway University of London, Egham, UK, [2]School of Environmental Sciences, University of East Anglia, Norwich, UK, [3]Centre for Atmospheric Science, University of Cambridge, Cambridge, UK, [4]National Centre for Atmospheric Science, Cambridge, UK, [5]Centre for Ecology and Hydrology, Penicuik, UK, [6]Facility for Airborne Atmospheric Measurements, Cranfield University, Cranfield, UK, [7]School of Earth, Atmospheric and Environmental Sciences, University of Manchester, Manchester, UK, [8]Centre for Ecology and Hydrology, Wallingford, UK, [9]Climate Change Research, Finnish Meteorological Institute, Helsinki, Finland, [10]Department of Geological Sciences, Stockholm University, Stockholm, Sweden, [11]Thomas H. Gosnell School of Life Sciences, RIT College of Science, Rochester, New York, USA

Abstract Isotopic data provide powerful constraints on regional and global methane emissions and their source profiles. However, inverse modeling of spatially resolved methane flux is currently constrained by a lack of information on the variability of source isotopic signatures. In this study, isotopic signatures of emissions in the Fennoscandian Arctic have been determined in chambers over wetland, in the air 0.3 to 3 m above the wetland surface and by aircraft sampling from 100 m above wetlands up to the stratosphere. Overall, the methane flux to atmosphere has a coherent $\delta^{13}C$ isotopic signature of $-71 \pm 1‰$, measured in situ on the ground in wetlands. This is in close agreement with $\delta^{13}C$ isotopic signatures of local and regional methane increments measured by aircraft campaigns flying through air masses containing elevated methane mole fractions. In contrast, results from wetlands in Canadian boreal forest farther south gave isotopic signatures of $-67 \pm 1‰$. Wetland emissions dominate the local methane source measured over the European Arctic in summer. Chamber measurements demonstrate a highly variable methane flux and isotopic signature, but the results from air sampling within wetland areas show that emissions mix rapidly immediately above the wetland surface and methane emissions reaching the wider atmosphere do indeed have strongly coherent C isotope signatures. The study suggests that for boreal wetlands ($>60°N$) global and regional modeling can use an isotopic signature of $-71‰$ to apportion sources more accurately, but there is much need for further measurements over other wetlands regions to verify this.

1. Introduction

Currently, there is a major gap between global methane (CH_4) budgets derived from "bottom-up" estimates (inventories) and budgets estimated from "top-down" observation such as those derived from global or regional inverse models [*Saunois et al.*, 2016; *Kirschke et al.*, 2013; *Nisbet and Weiss*, 2010]. Accurate source partitioning would help to understand and close that gap. Many inverse models only calculate net methane emissions (sources − sinks). Most inverse models that divide the methane emissions into different categories rely only on methane mole fraction measurements which means that only geographic locations of sources can be identified, not the nature of those sources. If two large different sources are closely juxtaposed (e.g., wetlands and gasfields), then apportionment can be problematic [*Bruhwiler et al.*, 2014; *Tsuruta et al.*, 2016].

The most powerful information available to improve source apportionment is isotopic. Methane sources such as wetlands, gas leaks, and biomass burning have widely different C isotopic ratios [e.g., *Schwietzke et al.*, 2016]. In principle, atmospheric measurements of these isotopic signatures can be used to apportion emissions from different source categories [*Hein et al.*, 1997; *Mikaloff Fletcher et al.*, 2004; *Bousquet et al.*, 2006; *Monteil et al.*, 2011; *Kai et al.*, 2011; *Levin et al.*, 2012]. This is only possible if isotopic signatures of

emissions can be shown to be coherent across specific source categories. This is not self-evident. Within source categories there are often wide temporal and geographic variations in the signature of the emission [e.g., *Zazzeri et al.*, 2016].

The mixing ratio of methane in the atmosphere has increased from a preindustrial value of 0.715 ppm [*Etheridge et al.*, 1998] to 1.833 ppm in 2014 (global mean [*WMO*, 2015]). Although most broad source types are known, there remains uncertainty in the contribution of different methane sources to the global methane budget [*Saunois et al.*, 2016]. As a result, interannual variations in the global methane growth rate are largely unexplained. Since 2007, following a period of 8 years of near stability, methane mole fractions have increased globally with a depletion in ^{13}C suggesting that this was caused by increasing biogenic sources [*Nisbet et al.*, 2014; *Schaefer et al.*, 2016]. Studies have suggested that the rise either is attributed to increased natural wetland emissions, initially due to warmer temperatures at northern high latitudes in 2007 and then later to heavy rainfall over tropical wetlands in 2008–2009 and 2010–2011 [*Dlugokencky et al.*, 2011; *Nisbet et al.*, 2014], or is a result of increased agricultural emissions [*Schaefer et al.*, 2016]. Studies of ethane and methane column measurements [*Hausmann et al.*, 2016] suggest that increased fossil fuel emissions have also significantly contributed to the methane rise.

Technological developments, particularly in laser spectroscopy systems which allow in situ measurements of methane mole fractions to high precision on platforms including ships, aircraft, and road vehicles, have helped to increase the number of measurements of methane mole fraction made in the Arctic, as well as other regions, in recent years. Thus, sources are being identified, e.g., emissions from surface waters of the Arctic Ocean [*Kort et al.*, 2012] and East Siberian Arctic Shelf [*Shakhova et al.*, 2014], which may be new, growing, or just not measured before.

Sources of methane in high northern latitudes include wetlands, permafrost and methane hydrate degradation, thermokarst lakes, marine emissions, forest fires, and natural gas leaks. Boreal and tundra regions contribute 3% to 10% of global methane emissions [*Olefeldt et al.*, 2012]. These emissions are likely to increase as the region warms. Emissions thought to have originated from degradation of submarine permafrost have been reported from the shallow East Siberian Arctic Shelf from shipboard observations (e.g., *Shakhova et al.* [2014]; see also *Berchet et al.* [2016] for constraints on the size of these emissions). Submarine gas plumes have been reported west of Spitsbergen [*Westbrook et al.*, 2009], although there is currently no evidence that the methane in these plumes reaches the atmosphere [*Fisher et al.*, 2011; *Lund Myhre et al.*, 2016], and in the south Kara Sea [*Portnov et al.*, 2013]. Methane emissions from ice-free areas of the Arctic Ocean up to 82°N have been recorded using aircraft measurements [*Kort et al.*, 2012]. As summer Arctic sea ice coverage decreases [*Comiso et al.*, 2008] emissions from the Arctic Ocean to the atmosphere are likely to increase.

Globally, natural wetlands constitute the largest source of methane to the atmosphere. Top-down studies suggest that there was an emission of 172 Tg CH$_4$ yr^{-1} from natural wetlands in 2012, 30% of the total global methane source of 568 Tg yr^{-1}, but there is a large range in the estimated wetland source, from 155 to 201 Tg CH$_4$ yr^{-1} [*Saunois et al.*, 2016]. Between 25 and 100 Tg CH$_4$ yr^{-1} is estimated to be from boreal and tundra biomes (>50°N) [*Olefeldt et al.*, 2012]. The large uncertainty in wetland emission estimates derives less from differences in the reported flux rates from specific habitat types [e.g., *Bartlett and Harriss*, 1993] but more from variability in reported wetland area, uncertainties in the seasonal and interannual variation in wetland area, wide variations in vegetation characteristics related to plant transport and oxidation of methane, and other factors causing variability in methane emissions which force large uncertainties when emissions are scaled up from the field to global [e.g., *Petrescu et al.*, 2010]. In addition, emissions from Arctic wetlands and subarctic shallow lakes can vary by a factor of 2 or more from one year to the next as a result of interannual meteorological changes [*Christensen*, 2014; *Thornton et al.*, 2015]. Satellite-based studies have suggested that emissions from Arctic wetlands are already increasing. In the period 2003 to 2007, methane release from Arctic wetlands (>67°N) is reported to have increased by 30.6 ± 0.9% [*Bloom et al.*, 2010]. Pan-Arctic methane emissions for the end of the 21st century forecasted by *Chen et al.* [2015] are 42% higher than they were for the period 1997 to 2006.

Methane emissions from wetland are dependent on temperature, water table, vegetation, and the microbial communities present [*McCalley et al.*, 2014]. Most previous studies of the isotopic composition of wetland methane have been process studies carried out using chambers. Chamber studies have shown that the

Table 1. Description of the Wetland Sites Studied

Site	Location	Wetland Type	Sampling Method	Mean Annual CH$_4$ Emission (g CH$_4$ m^{-2} yr^{-1}) in Other Published Studies
Sodankylä (Halssiaapa fen)	67°22.12′N, 26°39.24′E	Open eutrophic flark fen; abundant sedge vegetation, narrow ridges of birch trees	6 diel studies, 12 chambers	
Lompolojänkkä	67°59.83′N, 24°12.55′E	Open, nutrient-rich sedge fen; shrubs and sphagnum dominate	2 diel studies	20.5 [Lohila et al., 2016]
Kaamanen	69°08.43′N, 27°16.19′ E	Mesotrophic fen, aapa-type mire	3 diel studies	5.5 [Hargreaves et al., 2001]
Faerdesmyra	6943.96′N, 29°17.82′E	Palsa mire around Lake Ferdesvatnet	1 diel study	
Stordalen Mire (Abisko)	Site A: 68°21.35′N, 19°02.95′E; Site B: 68° 21.25′N, 19°02.87′E; Site C: 68°21.33′N, 19° 02.70′ E	Discontinuous permafrost; dry hummocks underlain by permafrost, wet depressions mostly colonized by sphagnum moss and minerotrophic wet areas, containing tall graminoid species	4 diel studies (at 3 locations) 46 chambers	27 [Jackowicz-Korczyński et al., 2010]

production pathway, transport, and oxidation of methane from wetlands can vary according to the temperature, water table, and vegetation type, with flux and isotopic signatures varying from one chamber to the next and from one wetland to another nearby [Chasar et al., 2000; Whiticar et al., 1986; McCalley et al., 2014]. Emissions are highly seasonal, with the strongest dependence on surface temperature [Worthy et al., 2000; Pickett-Heaps et al., 2011; Yvon-Durocher et al., 2014]. The largest influence on the isotopic composition of the emitted methane is whether the methane production pathway is via CO_2 reduction, producing methane highly depleted in ^{13}C (−110 to −60‰), or acetoclastic fermentation, generally producing methane more enriched in ^{13}C (−65 to −50‰) [Whiticar et al., 1986]. The path the methane takes, i.e., ebullition, transport through plants, or diffusion through the soil, affects the amount of oxidation of methane before ultimate emission to the atmosphere and thus also the isotopic composition of emitted methane. Methanogenesis produces methane depleted in ^{13}C, whereas microbial oxidation (methanotrophy) strongly fractionates to cause enrichment in ^{13}C of the remaining methane [Cicerone and Oremland, 1988]. Vascular plants can act as a conduit for the transport of methane from anoxic zones in sediment directly to the atmosphere without passing through oxic zones at the surface of the sediment. Methane generated in wetland sediments will be very depleted in ^{13}C, and some of this gas may escape with little fractionation via plant stalks and transpiration, while neighboring bubbles may encounter active methanotrophy and the residual methane that eventually reaches the atmosphere will be much richer in ^{13}C. Conversely, oxygen can be transported down through plants and be released, allowing methane oxidation to occur near the roots. Thus, species and amount of vegetation cover affects both emission rates [Strom et al., 2003; Kao-Kniffin et al., 2010] and isotopic composition of emitted methane [e.g., Chasar et al., 2000].

In water and plants, variable transport processes tend to produce varied isotopic signatures on very local scales. When this methane reaches the atmosphere integrative mixing immediately takes place. Thus, it is reasonable to consider the hypothesis that fine-scale variation in source signatures is lost and that an "average wetland isotopic signature" can be defined and that isotopic signatures (e.g., for "Arctic wetland") can be used for isotopic modeling on regional and global scales in order to discriminate sources by type.

This study presents measurements from the Methane and other greenhouse gases in the Arctic—Measurements, process studies and Modelling (MAMM) project campaigns of 2012 and 2013 which incorporated ground and aircraft
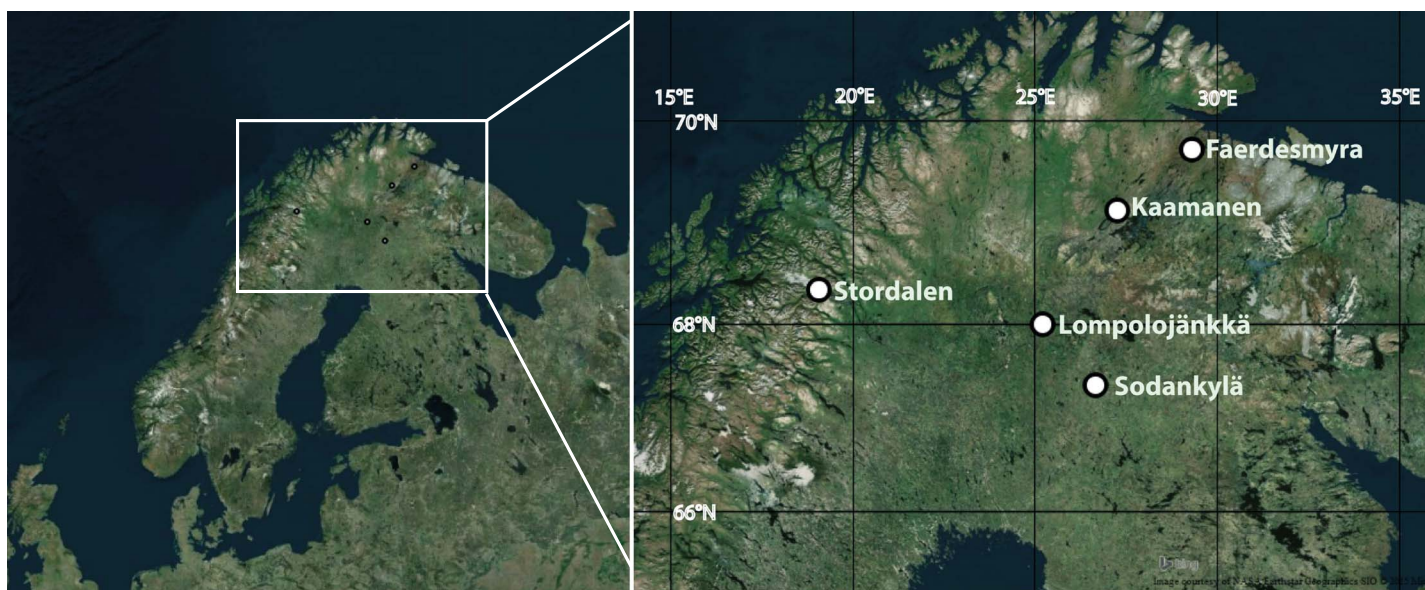
Figure 1. Map showing the location of the ground-based sampling sites. Mapped using QGIS 2.2.0 with basemap layer from Bing maps.

sampling of methane for isotopic analysis across northern Fennoscandia. To test the hypothesis that a coherent isotopic signature can be identified from specific wetlands, we studied wetlands on three different scales: (1) chamber studies at the soil, vegetation, and water-air interface; (2) air collection in open air at 30 cm and 3 m above the wetland surface in diel studies; and (3) air sampling by aircraft above wetlands in northern Finland and Sweden.

2. Measurements and Methodology

2.1. Study Sites

2.1.1. Ground Sites

Land cover in the study region is dominated by forest and peat bogs [*O'Shea et al.*, 2014]. Anthropogenic methane emissions across the study area are low. The EDGAR 4.2 methane inventory for 2008 gives a mean annual anthropogenic emission of 4.4 (±3.5, 1σ) tons of methane per $0.1° \times 0.1°$ grid square for the region enclosed between 67 to 70°N and 20 to 30°E [*EC-JRC/PBL*, 2011]. This mean anthropogenic emission is equivalent to 0.10 (±0.08, 1σ) g $CH_4 m^{-2} yr^{-1}$, around 2 orders of magnitude smaller than fluxes from wetlands in the region (as reported by *O'Shea et al.* [2014] and in Table 1). Figure 1 shows the locations of the five wetlands at which isotopic composition of methane emissions were measured in ground-based sampling campaigns: Sodankylä, Lompolojänkkä, and Kaamanen (all in Finland), Faerdesmyra (Norway), and Stordalen Mire (Sweden). Further details of the sites are given in Table 1. Diel sampling of ambient air (at 2 h intervals over a 24 h period) was carried out at each of these sites during the summer or early autumn of 2012 and 2013. Diel sampling was carried out at three different sites at Stordalen Mire in the summer of 2013. Site A was between lake and open mire, Site C (180 m WSW of site A) was in open mire, and samples at site B (190 m SSW of site A) were collected from within an area of tall graminoid plants where methane flux is known to be higher than from other parts of the mire [*Jackowicz-Korczyński et al.*, 2010]. Chamber sampling was also carried out at Sodankylä and Stordalen Mire. The sampling dates at each of the sites are listed in Table 2 (section 3).

2.1.2. Aircraft Sampling

The aircraft measurements reported in this paper were carried out as part of the MAMM project using the Facility for Airborne Atmospheric Measurement (FAAM) BAe 146 research aircraft. Three campaigns took place: 20 to 23 July 2012, 15 to 19 August 2013, and 19 to 23 September 2013 with flights from Kiruna in northern Sweden. This paper focuses on 11 flights (listed in Table 3) which were all above wetland regions of northern Fennoscandia. Flight paths are shown in the supporting information (Figure S2).

Table 2. Sampling Dates and Methane Isotopic Signatures Calculated From the Keeling Plots of Diel Measurements at the Wetland Sites

Wetland Site	Dates Sampled	δ^{13}C (‰)
Sodankylä	17–18 Jul 2012	−69.2 ± 0.6
	21–22 Jul 2012	−71.2 ± 1.6
	24–25 Jul 2012	−72.1 ± 2.0
	17–19 Aug 2013	−72.5 ± 1.0
	7–8 Sep 2012	−74.8 ± 0.9
	03–04 Oct 2013	−78.1 ± 0.8
Lompolojänkkä	18–19 Jul 2012	−72.3 ± 3.2
	7–8 Sep 2012	−68.0 ± 0.6
Kaamanen	22–23 Jul 2012	−71.7 ± 0.4
	15–16 Aug 2013	−68.0 ± 1.2
	9–10 Sep 2012	−74.0 ± 2.1
Faerdesmyra	23–24 Jul 2012	−72.0 ± 1.1
Stordalen Mire		
A	15–16 Aug 2013	−68.6 ± 0.1
B	19–20 Aug 2013	−59.6 ± 0.7
B	01–02 Jul 2014	−63.2 ± 0.6
C	01–02 Jul 2014	−69.8 ± 1.8

2.2. Air Sampling

2.2.1. Chamber Sampling

Chambers were deployed at Sodankylä in the summer of 2012 and Stordalen Mire in summer 2013. The chambers were constructed and installed by the Centre for Ecology and Hydrology [*Dinsmore et al.*, 2016]. Thirty-nine chambers were positioned over the wetland at Sodankylä (of which 12 were sampled for isotopic measurements in this study) and 46 at Stordalen Mire. The chamber locations were selected to be representative of the plant species across the site and within the footprint of eddy flux towers.

The chambers were constructed of opaque polypropylene pipe with a metal top. The lids were 25 cm tall, with a volume of ~30 L and covered an area of ground of 0.12 m^2 [*Drewer et al.*, 2010]. Four of the chambers at Stordalen Mire were taller (50 cm high) in order to enclose taller graminoids.

Chamber collars were installed to a depth of around 10 cm and left in position throughout the summer months.

The chamber lids were clipped to the collars with four bulldog clips when the measurements were made. A draught excluder made a leak tight seal between the collars and the chamber lids. Care was taken not to disturb the surrounding soil when the lids were connected, and all chambers were positioned close enough to a boardwalk to allow the person collecting samples to lean across from the boardwalk to avoid physically releasing methane bubbles by stepping on the ground.

Methane fluxes were calculated from measurement of the methane mole fraction change in the enclosed headspace. Four samples were collected by syringe throughout a 45 min incubation period (at 5, 15, 30, and 45 min) and transferred to 20 mL glass vials sealed with a rubber septum using a double-needle system [*Dinsmore et al.*, 2016]. Methane concentrations were measured by gas chromatography (HP5890 series II GC-FID) at the Centre for Ecology and Hydrology, Edinburgh, and fluxes calculated from either a linear or asymptotic best fit model for each chamber using GCflux, version 2 [*Levy et al.*, 2012].

Samples of air were also collected from each chamber for isotopic analysis. The chambers were closed for 45 min before a sample of air was collected from the chambers. The inlet of a microdiaphragm gas pump (KNF NMP830KNDC) operated by a 6 V battery was connected to a three-way valve on the chamber using flexible tubing. The valve to the chamber was opened, and the pump was run for 2 s to flush the tubing in the line with air from the chamber. A 1 L tedlar bag (SKC Ltd) was then connected to the outlet of the pump,

Table 3. Flight Dates and Times, Mixing Ratio Range, and Calculated Methane δ^{13}C Source Signatures[a]

Flight Number	Date	Time (UTC)	CH$_4$ Mixing Ratio Range (ppm)	Keeling Plot Intercept (‰)	Number of Samples	Keeling Plot Correlation (R)
B720	22 Jul 2012	10:55:28–16:08:35	1.865 to 1.900	−72.2 ± 3.3	31	0.908
B795	15 Aug 2013	14:05:28–17:39:00	1.859 to 1.890	−64.1 ± 1.9	24	0.955
B796a	16 Aug 2013	07:04:06–11:27:17	1.871 to 1.921	−72.2 ± 1.2	24	0.980
B796b	16 Aug 2013	13:34:05–17:32:20	1.873 to 1.927	−71.3 ± 1.5	22	0.944
B797	17 Aug 2013	05:45:56–10:16:12	1.851 to 1.961	−71.0 ± 0.6	25	0.992
B798	17 Aug 2013	12:03:51–16:23:33	1.850 to 1.922	−70.3 ± 1.4	16	0.944
B799	18 Aug 2013	07:05:09–11:52:21	1.867 to 1.930	−71.8 ± 2.1	23	0.924
B800	18 Aug 2013	12:57:13–17:59:56	1.859 to 1.891		20	0.715
B804	19 Sep 2013	14:46:17–18:04:32	1.912 to 1.938		19	0.569
B805	20 Sep 2013	06:08:05–09:43:04	1.871 to 1.909	−71.1 ± 4.5	19	0.838
B806	20 Sep 2013	11:17:14–15:45:51	1.894 to 1.940		23	0.501

[a]Results are from WAS bottle samples collected in the lowest 6.1 km (20,000 ft).

the valve on the bag opened, and air pumped into the bag from the chamber until approximately 800 mL of air filled the bag. Additionally, samples of ambient air were collected before the chambers were closed so that the change in mole fraction and isotopic composition of emitted methane could be calculated.

Twelve of the chambers in the wetland at Sodankylä were sampled for methane isotopic analysis at least twice in July 2012, and 46 chambers in the wetland at Stordalen Mire were each sampled three times: during the day between 10:15 and 17:00 (local time) on 18 August 2013, overnight between 01:45 and 03:11 on 19 August 2013, and during the day between 15:26 and 16:54 on 21 September 2013.

2.2.2. Ambient Air Sampling—Diel Cycles

Air samples were collected in 3 L Tedlar bags (SKC Ltd) from 30 cm and 3 m above ground level using a micro-diaphragm gas pump. Samples were collected every 2 h throughout 24 h periods, with samples collected from the two heights immediately after each other. The time taken to fill a bag was approximately 1 min. Overnight periods when low wind speeds and shallow boundary layer heights were forecast were preferred as these conditions allowed a large overnight buildup of methane. The sampling method was the same as that used in a previous study of the isotopic signature of emissions at Lompolojänkkä, Finland [*Sriskantharajah et al.*, 2012].

2.2.3. Aircraft Sampling

Methane mole fractions were measured at 1 Hz in real time throughout each of the flights using off-axis integrated cavity output spectroscopy (Fast Greenhouse Gas Analyzer (FGGA), Model RMT-200, Los Gatos Research Inc., USA). Details of the calibration and measurement uncertainty are given in the supporting information (Text S1) and by *O'Shea et al.* [2013].

Air samples were collected on board the FAAM aircraft using the Whole Air Sampling (WAS) system. Up to 64 flasks were installed in the aircraft hold on each flight. The WAS flasks are 3 L silica passivated stainless steel canisters (Thames Restek, UK). The flasks were evacuated prior to the flight and then filled to up to 3.25 bar using a double-headed stainless steel bellows pump (Senior Aerospace, USA) which pumped in air from the main sampling manifold of the aircraft. WAS flask filling software logged the times automatically. Fill times were selected based on the altitude of the aircraft and varied between 20 s at low altitude and 60 s at 9 km. Aircraft speed was usually 100 to 120 m/s, so low-altitude air sampling was representative of an integrated air sample over at least 2 km of ground track.

The times of sample collection were selected manually in response to the real-time onboard measurements of methane mole fraction by the FGGA in order to capture the range of mole fractions encountered on each flight.

2.3. Laboratory Analyses

All the WAS flask and Tedlar bag air samples were analyzed in the Greenhouse Gas Laboratory at Royal Holloway University of London. Methane mole fraction was measured using a Picarro 1301 cavity ringdown spectrometer (CRDS). Details of the calibration and measurement uncertainty are given in the supporting information (Text S1). The mean bias of the methane mole fractions measured in the WAS bottles by CRDS relative to the real-time FGGA measurements at the times the samples were collected was -0.5 (±4.6) ppb for the 400 samples collected on the 2012 and 2013 MAMM flights [*O'Shea et al.*, 2014]. The remainder of the air was kept for isotopic analysis.

If the measured methane mole fraction was greater than 8 ppm, the sample was diluted with zero-grade nitrogen until the mole fraction was in the range 1.7 to 8 ppm methane before isotopic analysis, giving measurement peak heights between 3.4 and 16 nA, over which range the isotopic response was linear. Methane $\delta^{13}C$ analysis was carried out using a modified gas chromatography isotope ratio mass spectrometry system for all samples (Trace Gas and Isoprime mass spectrometer, Isoprime Ltd.) with 0.05‰ repeatability [*Fisher et al.*, 2006]. All measurements for the WAS bottles and 3 L Tedlar bags were made in triplicate, but due to the small sample size just one measurement was made for the samples collected from the chambers. Each analysis used 75 mL of air. Isotope ratios are given in δ notation on the Vienna Peedee Belemnite scale.

2.4. Calculating Isotopic Source Signatures

Keeling plots [*Keeling*, 1958; *Pataki et al.*, 2003; *Sriskantharajah et al.*, 2012] were used to identify the isotopic source signature of the methane that was measured for the ambient air samples collected in both the ground-based (diel) and aircraft sampling campaigns. Using this technique, $\delta^{13}C$ of methane in each air sample is plotted against the reciprocal of the methane mole fraction. The *y* axis intercept and corresponding

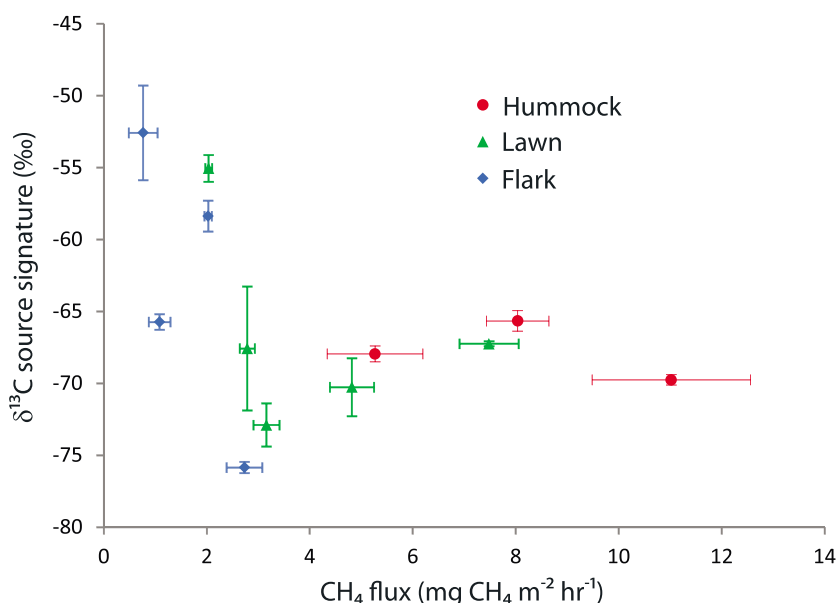**Figure 2.** Calculated δ^{13}C source signature and CH_4 flux measured in 12 chambers at Sodankylä. Chambers were categorized according to wetness: hummocks (red), lawns (green), and flarks (blue). The y axis error bars denote the standard error in calculated signature from two or three samples collected from each chamber on different days, between 20 and 26 July 2012. The x axis error bars denote the standard error in flux measurements carried out on 4 or 5 days between 20 and 26 July 2012.

uncertainty were calculated using a linear regression analysis which takes into account uncertainties in the x and y measurements as well as intrinsic scatter [*Akritas and Bershady*, 1996; *Zazzeri et al.*, 2015; *France et al.*, 2016]. The background concentration and isotopic composition (c_b and $\delta^{13}C_b$) do not necessarily need to be known. The y axis intercept represents the isotopic signature of the source of excess methane ($\delta^{13}C_s$) above background levels as shown by equation (1) (based on *Pataki et al.* [2003]).

$$\delta^{13}C_m = c_b\left(\delta^{13}C_b - \delta^{13}C_s\right) \times (1/c_m) + \delta^{13}C_s \tag{1}$$

where c_m and $\delta^{13}C_m$ are measured methane mole fraction and isotopic composition.

Isotopic source signatures for individual chambers were calculated using equation (2) if there was a methane increase of at least 0.05 ppm in the chamber during the 45 min that it was closed.

$$\delta^{13}C_s = \left(\delta^{13}C_{t1}c_{t1} - \delta^{13}C_{to}c_{to}\right) / (c_{t1} - c_{t0}) \tag{2}$$

where c_{t0} and c_{t1} are the methane mole fractions and $\delta^{13}C_{t0}$ and $\delta^{13}C_{t1}$ are methane isotopic compositions in samples collected at time t_o (before the chambers were closed) and t_1 (from the chamber after it was closed for 45 min).

2.5. Identifying Source Regions for Aircraft Measurements

Particle dispersion modeling using the UK Met Office NAME (Numerical Atmospheric-dispersion Modelling Environment) model was used to identify the regions that are likely to have contributed to the methane intercepted by the aircraft. NAME is a 3-D Lagrangian particle dispersion model [*Jones et al.*, 2007]. The UK Met Office's Unified Model meteorological fields were used. The model was run to identify backwards dispersion of air by modeling the release of 33,333 particles at the time and location of the WAS bottle collection and plotting the regions in which they were within the planetary boundary layer over the preceding 10 days as an integrated particle density.

3. Results

3.1. Chamber Measurements at Halssiaapa Fen, Sodankylä

The δ^{13}C of methane emitted from the chambers at Halssiaapa fen (Sodankylä) ranged from −76 to −53‰ (Figure 2). The methane in the chambers with the highest flux (>5 mg CH_4 m$^{−2}$ h$^{−1}$) corresponded to δ^{13}C in

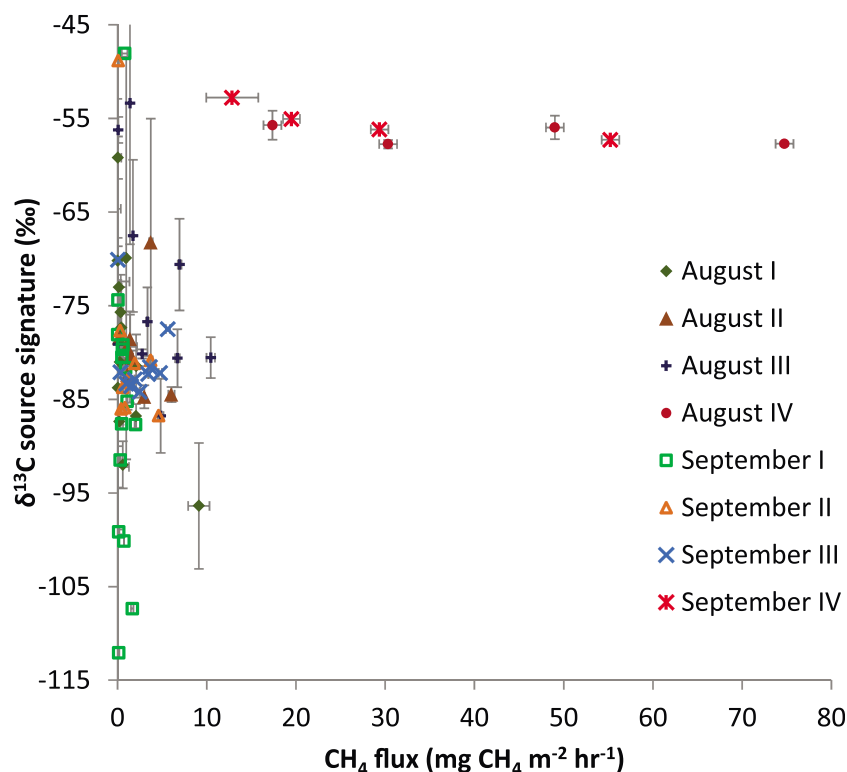**Figure 3.** Calculated δ^{13}C source signatures and fluxes for 41 chambers at Stordalen Mire in August 2013 and September 2013. Different colored symbols correspond to the four classes of chambers. Source signatures are only plotted if there was a >0.05 ppm increase in mole fraction in the chamber. The x error bars show the standard errors for flux measurements made on 18 August and 22 September. Some error bars are smaller than the symbol size. The y error bars for August show the standard error in two source signature calculation measurements for each chamber carried out on 18 and 19 August. The September isotope sampling was carried out on 21 September and was not repeated so error bars are not shown.

a tighter range between −70 and −66‰. A flux weighted mean δ^{13}C signature for the chambers was −68.0 ± 3.4‰. Equation (3) shows how the flux weighted mean δ^{13}C was calculated for *n* chambers, using the measured methane flux (*F*) and δ^{13}C values for each chamber.

$$\text{Flux weighted mean } \delta^{13}\text{C} = \frac{\sum_{i=1}^{n} F_i \, \delta^{13}C_i}{\sum_{i=1}^{n} F_i} \qquad (3)$$

Chambers were grouped according to wetness and vegetation cover into three categories: hummocks, lawns (*Sphagnum* dominated), and flarks (surface water) [*Laitenen et al.*, 2007]. From the subsample of chambers for which isotopic analysis was carried out, fluxes were higher from the hummocks, but there was no significant difference in isotopic signature between the categories (*P* values for an unequal variances *t* test were hummock/lawn, $P = 0.73$; flark/lawn, $P = 0.58$; and hummock/flark, $P = 0.43$). Mean signature for the hummock category was −67.8 ± 1.2‰ ($n = 3$), for lawn −66.6 ± 3.1‰ ($n = 5$), and for flark −63.1 ± 5.0‰ ($n = 4$).

The chambers in the hummock category covered deep-rooted sedge-type plants. These may have acted as a conduit of methane from deeper layers meaning high levels of methane can be emitted (despite lower water levels in these chambers) with little oxidation. The flux weighted mean δ^{13}C signature is weighted toward emissions from the hummock and lawn categories as these had the highest fluxes.

3.2. Chamber Measurements at Stordalen Mire

Flux measurements were made during the day on 18 August (Figures 3 and 4) and 22 September 2013 (Figure 3), and samples for isotope analysis were collected on 18 August (daytime), 19 August (nighttime), and 21 September (daytime). The δ^{13}C of methane emitted from the chambers at Stordalen Mire had a wide range from −112 to −48‰. Five of the 41 chambers at Stordalen in August and six in September had an
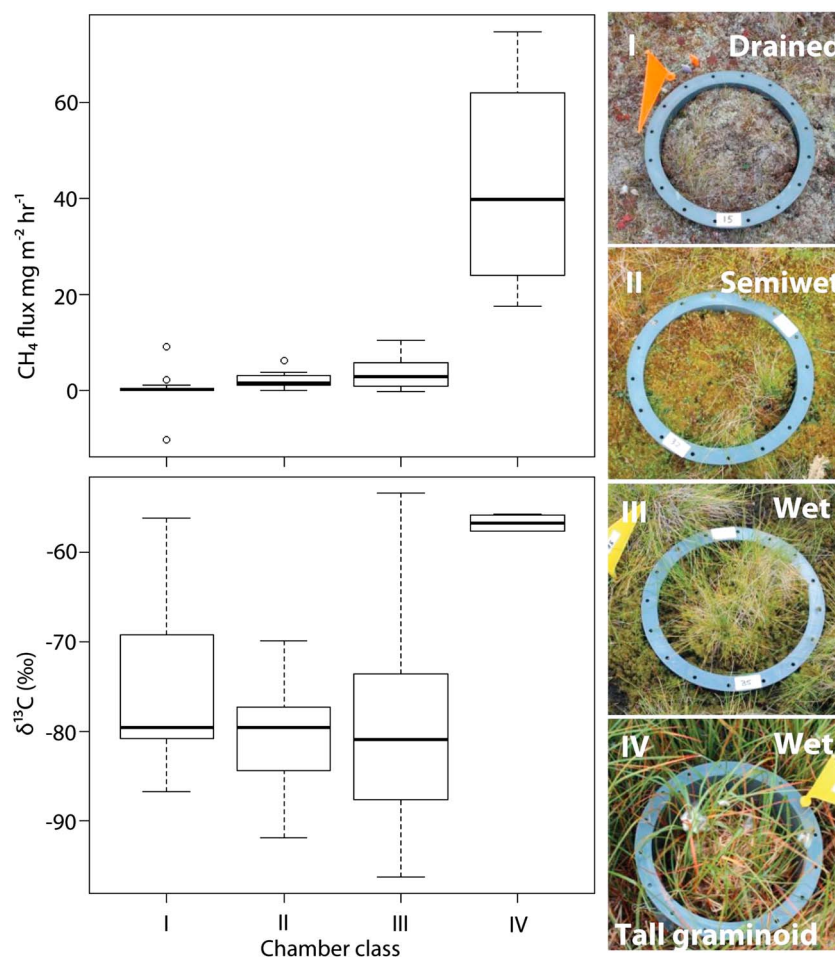
Figure 4. Box and whisker plot showing flux and δ^{13}C of emitted methane at Stordalen in August 2013 in each of four classes of chamber. Sampling for fluxes was carried out on 18 August and for isotopic measurement on 18 and 19 August. Examples of the four classes of chamber at Stordalen are shown in the photographs: I, Drained—Hummock and shrub; II, Semiwet—*Sphagnum* dominated; III, Wet—*Sphagnum* dominated; IV, Wet—tall graminoid (*Eriophororum angustifolium* dominated). There is no significant difference between δ^{13}C in categories I, II, and III ($P > 0.1$) but δ^{13}C in category IV is significantly higher than in all other categories ($P < 0.0001$).

increase in methane of less than 0.05 ppm during the 45 min that the chambers were closed so were not included in the source signature calculations. The chambers were categorized into four classes (I to IV) using the classification used by *Johansson et al.* [2006]: I Drained—Hummock and shrub; II Semiwet—*Sphagnum* dominated; III Wet—*Sphagnum* dominated; IV Wet—tall graminoid (*Eriophororum angustifolium* dominated) as shown in Figure 4. The four chambers in class IV had a much higher methane flux than the others. These were all situated in a small wet area dominated by tall *Eriophorum angustifolium* (cottongrass). In August the isotopic signature of methane from these four chambers was tightly constrained with a mean value of -56.8 ± 0.5‰, significantly more enriched than the mean value measured in the other chambers, -77.9 ± 1.6‰ ($P = 3 \times 10^{-15}$). The other three classes of chambers could not be isotopically distinguished from each other. The dry peats (class I) tended to have the lowest fluxes or uptake of methane by the drained peat. There was no evidence of a difference in isotopic composition between daytime and nighttime emissions. In September the four chambers in class IV again had the highest methane flux with a mean isotopic signature of -55.3 ± 1.0‰. This was also more enriched than the mean signature of emissions from the other chambers, -82.8 ± 2.1‰ measured at the same time ($P = 2 \times 10^{-13}$).

At Stordalen Mire the different habitat types have distinct local hydrology and nutrient statuses that result in highly variable emissions, so calculation of a flux weighted mean for these chambers is complicated. The methane fluxes measured from the four chambers in class IV in this study are significantly larger than
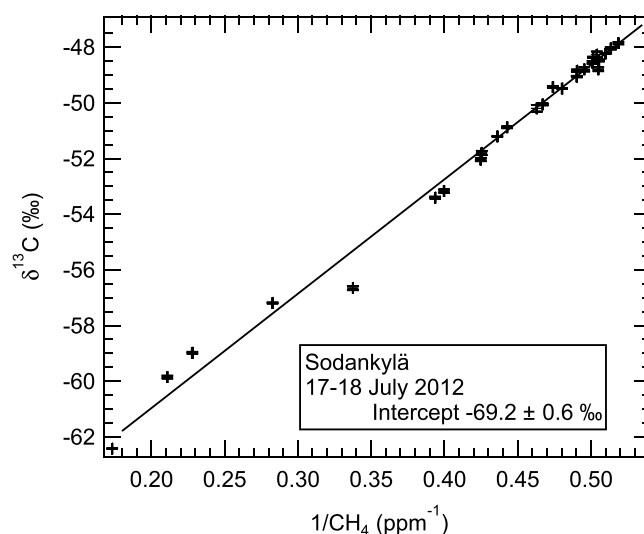
Figure 5. Keeling plot for air samples collected at 0.3 and 3 m above ground level in the Sodankylä fen, 17–18 July 2012.

fluxes measured from class IV at other parts of Stordalen in previous studies. *Johansson et al.* [2006] compiled tables of methane fluxes averaged over the growing season for each class and the area of each class at the site in 2000. The flux for class IV was $0.22\,g\,m^{-2}\,d^{-1}$ ($9.2\,mg\,m^{-2}\,h^{-1}$), 4 times smaller than the August flux shown in Figure 4. The larger flux in our study may in part be because the measurements were during peak emission periods and may be lower at other parts of the season or could reflect the large variability in emissions across this class. Class IV covers a much smaller area of the mire than the combined area of classes I, II, or III [*Johansson et al.*, 2006]. If the fluxes and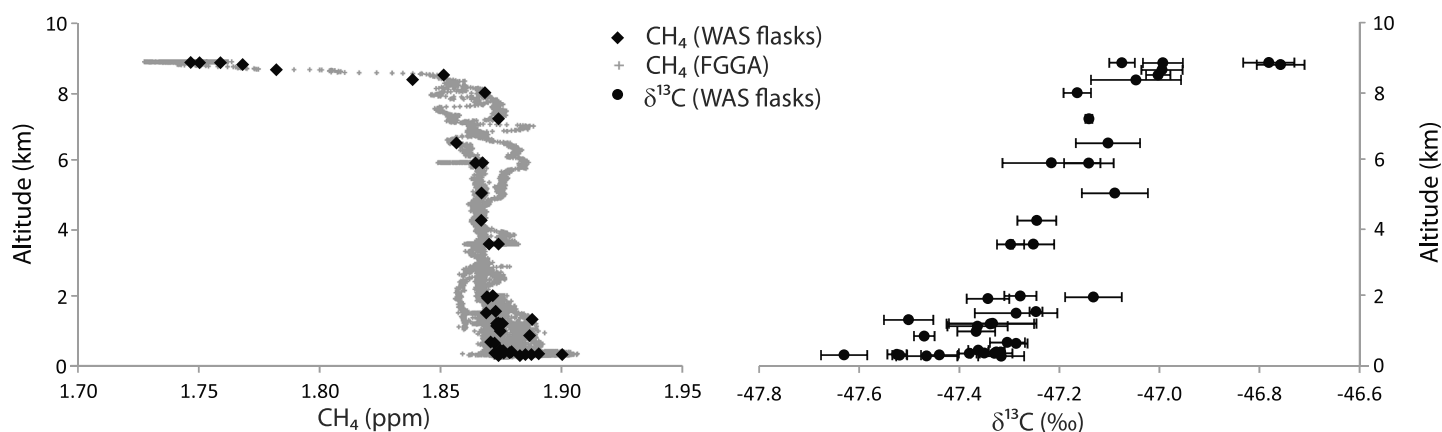 land areas of the four classes that were used by *Johansson et al.* [2006] are used together with the isotopic compositions from Figure 4 to calculate a flux weighted isotopic mean for the wetland, an isotopic composition of −69‰ is estimated, comparable to the diel measurements at sites A and C at Stordalen. If the relatively higher fluxes for class IV that were used in Figure 4 are used, then the flux weighted mean for the wetland is −61‰ (supporting information Table S1). A new estimation of the land cover in a circle of radius 300 m from site A was carried out using WorldView-2 satellite imagery (WorldView-2, 2013, https://www.digitalglobe.com/about/our-constellation, accessed 2017-03- 23) with segmentation classification carried out using the IDRISI Selva 17.0 package (see supporting information Figure S3). Within this area the proportions of land cover were estimated as 53% bog, 26% water, 14% *Eriophorum*, 5% shrubs, and 2% rock, confirming that the area covered by class IV vegetation (*Eriophorum*) is relatively small. The large proportion of the area covered by water should be noted. Transport of methane from wetland surface water to the atmosphere can be a large emission source, particularly during nighttime thermal convection [*Poindexter et al.*, 2016]. Measurement of the isotopic composition of methane emitted from the water would be required for scaling up the total amount of methane emitted from across the site (i.e., to compare with what is measured in ambient air sampling) as the lakes have a significant but highly variable methane bubble flux of around $0.56\,mg\,CH_4\,m^{-2}\,h^{-1}$ [*Wik et al.*, 2013].

3.3. Diel Measurements in Ambient Air at Five Wetland Sites

Table 2 lists the Keeling plot intercepts for each diel study. An example of one of these Keeling plots for the Sodankylä fen is shown in Figure 5 (see also supporting information, Figure S1) from which an isotopic source signature of −69.2 ± 0.6‰ was calculated. If separate Keeling plots are made for 0.3 m height and 3 m height the calculated source signatures are not significantly different: −68.9 ± 0.5‰ and −70.4 ± 1.5‰, respectively, for this example. In July and August the isotopic signatures are very consistent for all sites except Stordalen Mire, ranging from −68.0 to −72.5‰. Site B at Stordalen Mire had a Keeling plot intercept significantly higher than at all other sites (−59.6 ± 0.7‰ in August). This was the location of the tall graminoid plants (*Eriophorum angustifolium*) where chambers had high fluxes with methane more enriched in ^{13}C than at the other sites (−56.8 ± 1.1‰ in August and −55.3 ± 1.9‰ in September). The isotopic signature calculated at sites A and C is more likely to be representative of bulk emissions from the wetland, a mix of fen, bog, and pond emissions.

The isotopic source signature at the Sodankylä fen was consistent in July and August at −71.3 ± 1.5‰ but more depleted in ^{13}C in September (−74.8 ± 0.9‰) and October (−78.1 + 0.8‰). A previously published study at Lompolojänkkä [*Sriskantharajah et al.*, 2012] showed that methane emitted in May following the spring thaw was more enriched in ^{13}C than methane emitted later in the summer. These results suggest that there may be some seasonal variability, but further measurements throughout the spring and autumn would be required to confirm this.

Figure 6. Variation in methane mole fraction (measured using the FGGA on board the aircraft and in WAS flasks) and $\delta^{13}C$ (measured in WAS flasks) on flight B720 on 22 July 2012.

3.4. Aircraft Measurements

During flight B720 on 22 July 2012 the aircraft flew in a box pattern above Sodankylä from 100 m to 9000 m above ground. A plot of the measured mole fraction and isotopic composition of methane is shown in Figure 6. This flight was carried out on the same day as ground-based sampling at the site. A detailed study of this flight including calculations of the methane flux from the wetlands has been published separately [*O'Shea et al.*, 2014] showing that the regional average methane flux from the wetlands was $1.2 \pm 0.5 \, mg \, CH_4 \, h^{-1} \, m^{-2}$ on that day.

There was a sharp drop in methane mixing ratio in one sample at 6.6 km and in all samples above 8.4 km as stratospheric air was measured. Methane in most air sampled above 8.4 km was also relatively enriched in ^{13}C. The highest sample, collected in the lower stratosphere at 9 km altitude, had a methane mole fraction of 1.747 ppm and $\delta^{13}C$ of -46.78 ± 0.05‰. A sharp enrichment in $\delta^{13}C$ due to the kinetic isotope effect during methane sink reactions as methane mole fraction drops in the stratosphere was expected and has been seen in other studies [e.g., *Rice et al.*, 2003; *Röckmann et al.*, 2011; *Sugawara et al.*, 1997].

A source signature of -72.2 ± 3.3‰ is calculated from the Keeling plot intercept of all measurements in the lowest 6.1 km for flight B720. This maximum altitude of 6.1 km was selected to ensure that there was no stratospheric influence.

The largest methane mole fractions were recorded on flight B797 on 17 August 2013. The in situ measurements of methane mole fraction throughout this flight are shown in Figure 7 along with the locations of WAS bottle collection. The Keeling plot in Figure 8 for flight B797 was based on measurements in these WAS bottles.

Table 3 lists the isotopic signatures calculated for each flight over the wetland region, and Figure 8 shows the corresponding Keeling plots that were produced for each flight. The strongest correlations between $\delta^{13}C$ and $1/CH_4$ and largest mole fraction ranges were obtained in flights B796a, B796b, B797, B798, and B799 in August 2013, and the Keeling plot uncertainties were lowest for these flights. The correlation between $\delta^{13}C$ and $1/CH_4$ was weak ($P > 0.01$) for flights B804 and B806 (September 2013), so they have been excluded from the analysis. B800 has also been excluded because the sample with lowest concentration was far from the regression line and the regression had a large uncertainty (± 7.9). These flights may have been influenced by local emissions that had not been well mixed.

An atmospheric dispersion model, NAME, is used to investigate whether the air sampled on the flights had recently passed over known wetland regions. Figure 9 shows footprint maps for each of the flights in Table 3. These footprints are composites generated from all of the WAS locations for each flight. They show an overall region of influence for each of the flights.

Inspection of Figure 9 shows that the flight with the largest enhancement in methane, B797, has a footprint with a relatively large influence from the surface. Close to the WAS locations in the PBL, there is a high density
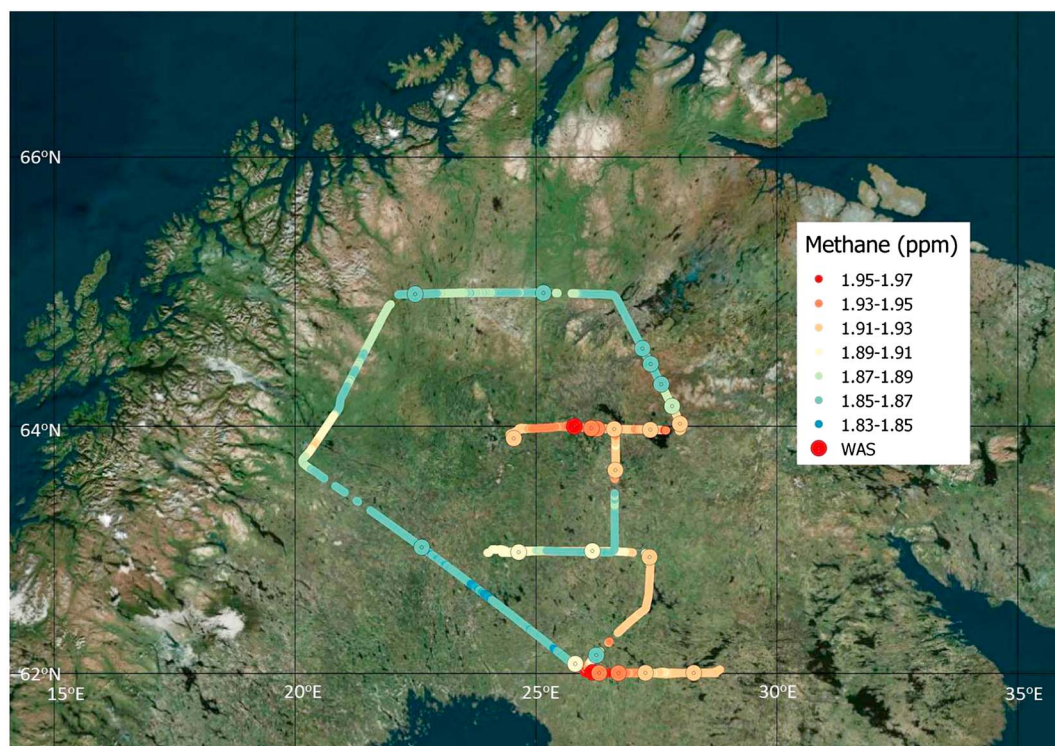
Figure 7. Map of methane mole fraction measured on the FGGA and in WAS bottles collected on flight B797 on 17 August 2013. Mean difference (WAS mole fraction − FGGA mole fraction) was −1.2 ppb, within the FGGA measurement uncertainty. Mapped using QGIS 2.2.0 with basemap layer from Bing maps.

of modeled particles, as indicated by the widespread darker blue colors. This means that the sampled air had recently spent more time in the PBL than many of the other flights, over a region to the northeast of the Bay of Bothnia where wetlands are located [*Melton et al.*, 2013]. The flights with the larger methane enhancements (Table 3) had footprints with highest particle densities over wetland regions in Finland, Sweden, Russia, and Norway. Wetlands are the largest source of methane in these areas, as there are few anthropogenic sources. *O'Shea et al.* [2014] show the European Environment Agency's Corine land cover database map [*Corine*, 2014] over approximately 20°E to 28°E and 66°N to 69.5°N, which contains Kaamanen and Sodankylä, and note that the largest land types by area are forests followed by peat bogs (23% over the area shown).

Flights with smaller methane enhancements tended either to have more influence from over the sea, for example B800, or to have a smaller footprint altogether, for example, B804 and B805. The footprint on B797 indicates lower wind speeds in the PBL, so the air was able to pick up local wetland methane emissions over a longer time period. In contrast, the higher wind speeds in B804 mean that although the air passed over some wetland areas, there was less time for the emissions to mix up into the air mass. A more comprehensive modeling study would be required to fully resolve the sources contributing to the enhancements on each of the flights. However, this qualitative analysis is consistent with the hypothesis of wetlands being the main source of methane in these flights.

4. Discussion

4.1. Scaling Up From Chamber Measurements to Regional Isotopic Signatures

The wide range in $\delta^{13}C$ of the methane emitted into chambers, from −53 to −76‰ at the Sodankylä fen and −48 to −112‰ at Stordalen Mire, reflects the heterogeneity of wetland methane emissions. At Sodankylä the source signature of the chambers with the largest methane fluxes, greater than $5\,mg\,CH_4\,m^{-2}\,h^{-1}$, was tightly clustered around -68 ± 2‰. The study at Sodankylä considered the variation between 12 chambers, but to accurately calculate the isotopic signature of methane emitted to the atmosphere, many more
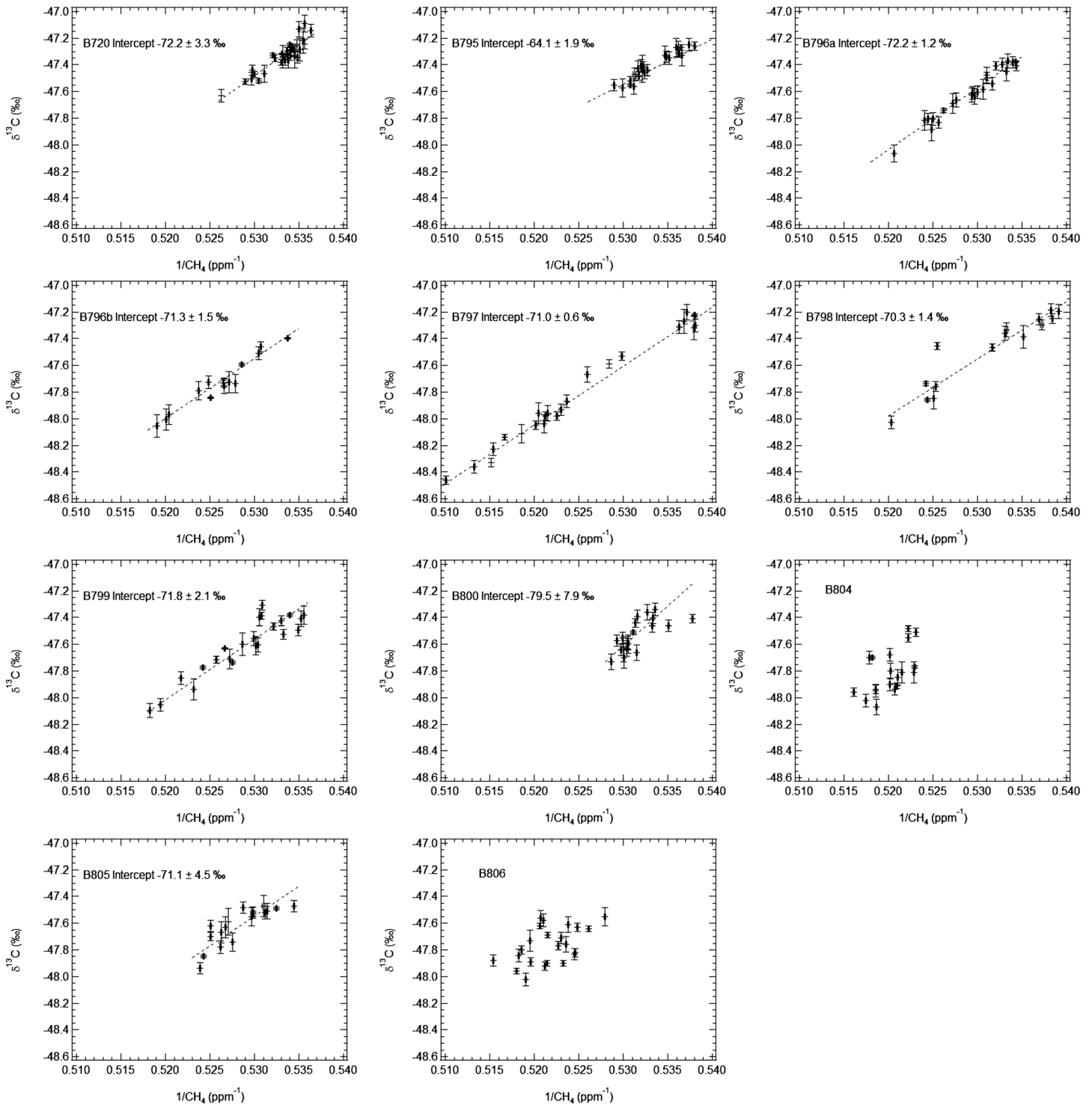
Figure 8. Keeling plots for WAS bottles collected on all flights. The y axis intercepts denote the source isotopic compositions.

chambers would be required. Within a particular chamber there can be changes in the isotopic signature of the emitted methane, even within a short time period. Differences of up to 8.6‰ at Sodankylä and up to 30.4‰ at Stordalen Mire were seen in the isotopic signatures in repeat sampling taken from the same chambers in the same week. This could be due to differences in the emission process (e.g., amount of ebullition) during the time the chambers are closed.
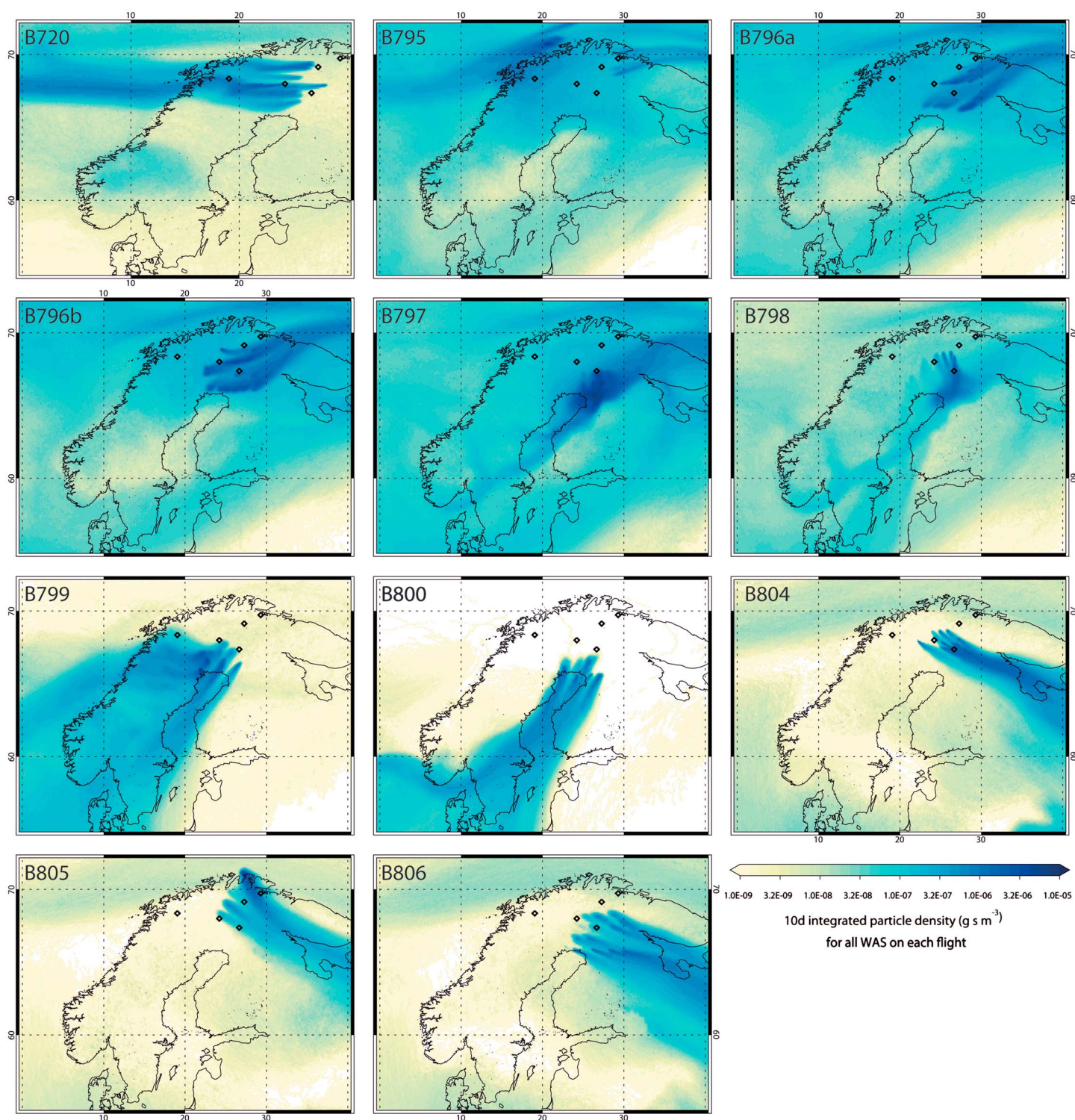
Figure 9. NAME plots for each flight. The maps show composite footprints for all WAS bottles collected on each flight. The dots show the locations of the five ground study sites.

The study at Stordalen showed that methane fluxes were much higher from the chambers located in a wet area over tall graminoid (*Eriophorum angustifolium*) plants than in *Sphagnum*-dominated areas and that the isotopic composition of emissions was significantly more enriched in ^{13}C from the chambers over *Eriophorum angustifolium*. Increased methane fluxes in areas dominated by *Eriophorum angustifolium* due to the vascular

Table 4. Summary Table of Mean Methane $\delta^{13}C$ Isotopic Signature of Wetland Emissions for July, August, and September Derived From Sampling of Ambient Air in Diel Studies in Wetlands and in the Aircraft Campaigns

	Wetland Site	Source $\delta^{13}C^a$ (‰)
Diel studies	Sodankylä	−72.0 (5)
	Lompolojänkkä	−70.2 (2)
	Kaamanen	−71.2 (3)
	Faerdesmyra	−72.0 (1)
	Stordalen (sites A and C)	−69.2 (2)
	Mean $\delta^{13}C$ signature (diel)	−70.9 (13)
	1σ	1.2
Aircraft studies	Mean $\delta^{13}C$ signature (aircraft)	−70.5 (8)
	1σ	2.7

aNumber of studies in parentheses.

plants being more productive [e.g., *Bäckstrand et al.*, 2010] and providing a conduit for methane transport from the rhizosphere to the atmosphere [*Öquist and Svensson*, 2002] has been observed in previous studies at Stordalen Mire, although the measured emissions in this study were larger than the emissions published previously. *Eriophorum angustifolium* was not present at Sodankylä which explains the absence of such large fluxes in the chambers at Sodankylä. The isotope results are supported by a recent study by *McCalley et al.* [2014] at Stordalen Mire, who using autochambers and measurements by a quantum cascade laser in summer 2011 identified an isotopic signature of −79.6 ± 0.9‰ at a *Sphagnum* site and −66.3 ± 1.6‰ at an *Eriophorum angustifolium* site. These chamber studies have been shown to be useful for determining how different plant species and methanogenic communities affect the emitted methane. The Stordalen Mire studies have demonstrated that even with a large number of chambers it is difficult to calculate an expected isotopic signature for the whole wetland area using chamber measurements because the signatures and fluxes are so variable. Chamber studies may show wide variations in very close proximity, depending on the presence or absence of methane transport by plants, subtle changes in hydrology or pH, microbial community structure, or vigor of local methanotrophy. The chamber approach therefore requires large numbers of chambers whose measurements should be spatially weighted to provide a comparable flux and statistically linked isotopic signature to aboveground eddy covariance/isoflux measurements [e.g., *Santoni et al.*, 2012; *Marushchak et al.*, 2016].

Keeling plots can be justifiably used for identification of the source signature during periods when there is a consistent background mole fraction and isotopic composition to which there is an increment of methane added from a uniform source or source mix. This was possible for the diel studies which were carried out under still conditions, usually with lowest methane mole fraction measured in the afternoon, increasing overnight as emissions from the local wetland built up under the boundary layer. The diel measurements were able to provide a more tightly constrained isotopic signature for methane from each wetland area. The signature of summer (July, August, and September) emissions was between −68.0 and −72.5‰, with a mean value derived from averaging the means for the five sites of −70.9 ± 1.2‰ (Table 4).

The Keeling plot technique could also be used for aircraft measurements, when flying at low level close to the wetland source with a consistent prevailing wind. Continuous, real-time measurement of methane mole fraction on board the aircraft using the FGGA allowed samples to be collected in the WAS bottles for isotopic analysis across the whole range of methane levels seen on the flights.

By comparison of the source signature calculated for each flight with the isotopic signature calculated by the ground-based sampling, along with identification of the potential source area using NAME, we have confirmed that methane increases measured on these summer flights were from wetland emissions in northern Norway, Sweden, and Finland. The mean isotopic signature for the wetland flights was −70.5 ± 2.7‰. This agrees well with the mean of the summer signatures calculated from the wetland diel studies, −70.9 ± 1.2‰, and appears to be representative of the bulk emission from European Arctic wetlands in summer.

4.2. Comparison With Other Boreal Methane Emission Signatures

Northern Scandinavia is one of the best places to measure wetland $\delta^{13}C$ of methane in ambient air due to the lack of other large methane emissions from the region. Some other aircraft studies have been complicated by the presence of other large sources in the study areas, e.g., *Umezawa et al.* [2012]. The isotopic signature of −71‰ is similar to the signature of methane released in ebullition from northern Siberian lakes (−70‰ [*Walter et al.*, 2008]), wetland emissions in western Siberia (−70‰) [*Umezawa et al.*, 2012], and long-range transported methane to the Arctic from northern Russia [*France et al.*, 2016], suggesting that this isotopic

signature may be representative of boreal wetland emissions, but this should be verified by aircraft campaigns over other regions in which wetlands emissions dominate. New measurements in Canadian wetland regions have been made using the diel sampling technique for comparison (see supporting information). The isotopic signature of emissions was −66.8 ± 1.6‰ at East Trout Lake in Saskatchewan (Figure S4) and −67.2 ± 1.1 at Fraserdale in Ontario (Figure S5), both slightly more enriched in ^{13}C than the emissions from northern Scandinavian wetlands [*Miller et al.*, 2014; *Kuhlmann et al.*, 1998].

The wetland signature is distinct from emissions from many other Arctic sources such as gas deposits and marine and estuarine emissions. Values of between −55 and −34‰ have been reported for Siberian natural gas [*Cramer et al.*, 1999], and the signature of the mix of this gas that enters the distribution network is around −50‰ [*Lowry et al.*, 2001]. Methane in the Lena river estuary [*Bussmann*, 2013] has an isotopic signature of −34‰. Further measurements of isotopic signatures are needed for other Arctic methane sources to confirm whether wetlands can be systematically distinguished isotopically from other potentially large sources, e.g., subsea permafrost and hydrate releases and by ventilating surface waters in the East Siberian Arctic Shelf [e.g., *Shakhova et al.*, 2014; *Portnov et al.*, 2013].

Optimally, models should use different isotopic signatures for wetland emissions from different regions. Some studies report isotopic composition of methane in sediment and water [e.g., *Holmes et al.*, 2015], but the signature of methane actually emitted to the atmosphere is rarely measured. Methane from wetlands in other regions also needs to be better constrained. For example, there have been very few studies of the isotopic composition of methane from tropical wetlands.

High-latitude wetland emissions may be more depleted in ^{13}C than those from wetlands farther south, in part due to less oxidation of methane before it is emitted than in warmer wetlands which often have thicker oxic layers, in part due to differences in methanogenic communities and also because the precursor plant material is C3 which is more depleted in ^{13}C than the C4 plants that are abundant in the tropics. It should be noted that the isotopic signatures measured in this study are lower than those used in global models which may mean that a given emissions scenario in the models may underestimate the change to atmospheric δ^{13}C (as also discussed by *McCalley et al.* [2014]). Typically, global averaged wetland methane isotopic signatures are used in the models, e.g., −59‰ [*Monteil et al.*, 2011] or −58‰ [*Bousquet et al.*, 2006]. Using a more depleted value of δ^{13}C for the boreal wetland source has been shown to provide a better fit to atmospheric observations of methane δ^{13}C at high northern latitudes [*Warwick et al.*, 2016].

High-latitude wetland fluxes are highly seasonal with the largest proportion of the emissions from northern Fennoscandia occurring between May and October. At Lompolojänkkä emissions peak in July and August, with September emissions half of those in August [*Lohila et al.*, 2016]. The wetland source is visible in atmospheric methane δ^{13}C records measured at high-latitude atmospheric background stations as a late summer depletion in ^{13}C which contrasts with the more enriched signature typical of winter emissions from northern sources, e.g., gasfield emissions [*Fisher et al.*, 2011].

5. Summary

The results show that the isotopic signature for wetland emissions in the European Arctic is strongly depleted in ^{13}C compared with methane in the atmosphere, with a source signature of −71 ± 2‰ for northern European wetland emissions based on the FAAM aircraft and diel measurements during MAMM. Major increases in Arctic methane emissions from wetlands [e.g., *Chen et al.*, 2015] would produce a negative shift in regional and then global atmospheric $\delta^{13}C_{CH4}$ values. Further work is required to fully investigate whether this is representative of emissions from other Arctic regions, e.g., in Siberia and Canada, and whether there are regional differences in the seasonal variability of the isotopic signature of northern wetland emissions.

The study has compared isotopic signatures of wetland emissions calculated using three methods: using samples collected from chambers, diel variations in ambient air at ground level, and aircraft sampling throughout the troposphere. In each of the collection suites, isotopic source signatures could be calculated with a small uncertainty using the Keeling plot method. In comparison with mobile on-site isotopic measurement (e.g., by analyzers using optical techniques, excellent for "very near source" studies with high mole fractions), the off-line method is very successful in studies of isotopic signatures of emissions in *ambient* air masses—with easy collection and convincingly high precision.

The results show that it is indeed possible to define a summer boreal wetland regional isotopic signature for use in modeling methane emissions at regional and global scales. In contrast to the varied results from chambers, even as low as 3 m above the wetland the mixing in the local air masses had produced an integrated signature of -71 ± 1‰. At 100 m above the wetlands, the aircraft measurements showed the same signature over wide tracts of wetland in well-characterized air masses. This signature could also be identified in far-traveled air arriving after multiday transport at the remote Zeppelin station [*Fisher et al.*, 2011] and also sampled in air over the Arctic Ocean [*France et al.*, 2016] in air transported from Siberia. The Canadian diel results found that the methane was slightly more enriched at -67 ± 1‰, but these measurements were at lower latitudes (54°21′N and 49°53′N) on the southern fringe of the boreal forest. The value of -71 ± 1‰ could be used as a representative isotopic signature of wetland methane emissions from boreal regions at >60°N, although further diel and aircraft campaigns across wetlands farther north in Canada and Siberia should be carried out to verify this.

Many studies of methane emissions using chamber measurements in wetlands require scaling up from chamber collections to regional or even global scale: the difficulty of upscaling introduces large uncertainties both in derived fluxes of methane from wetlands and derived isotopic composition of the emitted methane. In contrast, the use of Keeling plot studies of air samples collected in open air radically simplifies the upscaling task. In particular, the aircraft measurements allowed the emissions on a regional scale to be isotopically characterized. The Keeling technique should also be suitable for determining regional isotopic signatures of methane emissions in large regions of tropical wetlands which are particularly poorly characterized.

To conclude, identification of coherent regional emissions signatures from wetlands should be possible and can be achieved by rapid in situ sampling. Such regional isotopic signatures can then be used to support the inclusion of isotopic measurements in global and regional models, constraining methane emissions with much better source apportionment.

References

Akritas, M. G., and M. A. Bershady (1996), Linear regression for astronomical data with measurement errors and intrinsic scatter, *Astrophys. J.*, 470(2), 706–714.

Bäckstrand, K., P. M. Crill, M. Jackowicz-Korczyński, M. Mastepanov, T. R. Christensen, and D. Bastviken (2010), Annual carbon gas budget for a subarctic peatland, northern Sweden, *Biogeosciences*, 7(1), 95–108, doi:10.5194/bg-7-95-2010.

Bartlett, K. B., and R. C. Harriss (1993), Review and assessment of methane emissions from wetlands, *Chemosphere*, 26(1–4), 261–320.

Berchet, A., et al. (2016), Atmospheric constraints on the methane emissions from the East Siberian Shelf, *Atmos. Chem. Phys.*, 16, 4147–4157, doi:10.5194/acp-16-4147-2016.

Bloom, A. A., P. I. Palmer, A. Fraser, D. S. Reay, and C. Frankenberg (2010), Large-scale controls of methanogenesis inferred from methane and gravity spaceborne data, *Science*, 327(5963), 322–325, doi:10.1126/science.1175176.

Bousquet, P., et al. (2006), Contribution of anthropogenic and natural sources to atmospheric methane variability, *Nature*, 443(7110), 439–443, doi:10.1038/Nature05132.

Bruhwiler, L., E. J. Dlugokencky, K. Masarie, M. Ishizawa, A. Andrews, J. Miller, C. Sweeney, P. Tans, and D. Worthy (2014), CarbonTracker-CH4: An assimilation system for estimating emissions of atmospheric methane, *Atmos. Chem. Phys.*, 14, 8269–8293, doi:10.5194/acp-14-8269-2014.

Bussmann, I. (2013), Distribution of methane in the Lena Delta and Buor-Khaya Bay, Russia, *Biogeosciences*, 10(7), 4641–4652, doi:10.5194/bg-10-4641-2013.

Chasar, L. S., J. P. Chanton, P. H. Glaser, and D. I. Siegel (2000), Methane concentration and stable isotope distribution as evidence of rhizospheric processes: Comparison of a fen and bog in the Glacial Lake Agassiz Peatland complex, *Ann. Bot.*, 86(3), 655–663, doi:10.1006/anbo.2000.1172.

Chen, X., T. J. Bohn, and D. P. Lettenmaier (2015), Model estimates of climate controls on pan-Arctic wetland methane emissions, *Biogeosciences*, 12, 6259–6277, doi:10.5194/bg-12-6259-2015.

Christensen, T. R. (2014), Climate science: Understand Arctic methane variability, *Nature*, 509(7500), 279–281.

Cicerone, R. J., and R. S. Oremland (1988), Biogeochemical aspects of atmospheric methane, *Global Biogeochem. Cycles*, 2, 299–327, doi:10.1029/GB002i004p00299.

Comiso, J. C., C. L. Parkinson, R. Gersten, and L. Stock (2008), Accelerated decline in the Arctic Sea ice cover, *Geophys. Res. Lett.*, 35, L01703, doi:10.1029/2007GL031972.

Corine (2014), Corine land cover 2006 raster data, European Environment Agency. [Available at http://eea.europa.eu/data-and-maps/data/clc-2006-raster-3, accessed 2016-12-06.]

Cramer, B., H. S. Poelchau, P. Gerling, N. V. Lopatin, and R. Littke (1999), Methane released from groundwater: The source of natural gas accumulations in northern West Siberia, *Mar. Pet. Geol.*, 16(3), 225–244, doi:10.1016/s0264-8172(98)00085-3.

Dinsmore, K. J., J. Drewer, P. E. Levy, C. George, A. Lohila, M. Aurela, and U. Skiba (2016), Growing season CH_4 and N_2O fluxes from a sub-Arctic landscape in northern Finland, *Biogeosci. Discuss.*, doi:10.5194/bg-2016-238.

Dlugokencky, E. J., E. G. Nisbet, R. Fisher, and D. Lowry (2011), Global atmospheric methane: Budget, changes and dangers, *Philos. Trans. R. Soc. A*, 369(1943), 2058–2072, doi:10.1098/rsta.2010.0341.

Drewer, J., et al. (2010), Comparison of greenhouse gas fluxes and nitrogen budgets from an ombotrophic bog in Scotland and a minerotrophic sedge fen in Finland, *Eur. J. Soil Sci.*, 61, 640–650, doi:10.1111/j.1365-2389.2010.01267.x.

EC-JRC/PBL (2011), Emission Database for Global Atmospheric Research (EDGAR), release version 4.2. [Available at http://edgar.jrc.ec. europa.eu.]

Etheridge, D. M., L. P. Steele, R. J. Francey, and R. L. Langenfelds (1998), Atmospheric methane between 1000 AD and present: Evidence of anthropogenic emissions and climatic variability, *J. Geophys. Res.*, *103*, 15,979–15,993, doi:10.1029/98JD00923.

Fisher, R., D. Lowry, O. Wilkin, S. Sriskantharajah, and E. G. Nisbet (2006), High-precision, automated stable isotope analysis of atmospheric methane and carbon dioxide using continuous-flow isotope-ratio mass spectrometry, *Rapid Commun. Mass Spectrom.*, *20*(2), 200–208, doi:10.1002/Rcm.2300.

Fisher, R. E., et al. (2011), Arctic methane sources: Isotopic evidence for atmospheric inputs, *Geophys. Res. Lett.*, *38*, L21803, doi:10.1029/2011GL049319.

France, J. L., et al. (2016), Measurements of $d^{13}C$ in CH_4 and using particle dispersion modeling to characterize sources of Arctic methane within an air mass, *J. Geophys. Res. Atmos.*, *121*, 14,257–14,270, doi:10.1002/2016JD026006.

Hargreaves, K. J., D. Fowler, C. E. R. Pitcairn, and M. Aurela (2001), Annual methane emission from Finnish mires estimated from eddy covariance campaign measurements, *Theor. Appl. Climatol.*, *70*, 203–213.

Hausmann, P., R. Sussmann, and D. Smale (2016), Contribution of oil and natural gas production to renewed increase in atmospheric methane (2007–2014): Top–down estimate from ethane and methane column observations, *Atmos. Chem. Phys.*, *16*, 3227–3244, doi:10.5194/acp-16-3227-2016.

Hein, R., P. J. Crutzen, and M. Heimann (1997), An inverse modeling approach to investigate the global atmospheric methane cycle, *Global Biogeochem. Cycles*, *11*, 43–76, doi:10.1029/96GB03043.

Holmes, M. E., J. P. Chanton, M. M. Tfaily, and A. Ogram (2015), CO_2 and CH_4 isotope compositions and production pathways in a tropical peatland, *Global Biogeochem. Cycles*, *29*, 1–18, doi:10.1002/2014gb004951.

Jackowicz-Korczyński, M., T. R. Christensen, K. Backstrand, P. Crill, T. Friborg, M. Mastepanov, and L. Strom (2010), Annual cycle of methane emission from a subarctic peatland, *J. Geophys. Res.*, *115*, G02009, doi:10.1029/2008JG000913.

Johansson, T., N. Malmer, P. M. Crill, T. Friborg, J. H. Akerman, M. Mastepanov, and T. R. Christensen (2006), Decadal vegetation changes in a northern peatland, greenhouse gas fluxes and net radiative forcing, *Global Change Biol.*, *12*, 2352–2369, doi:10.1111/j.1365-2486.2006.01267.x.

Jones, A., D. Thomson, M. Hort, and B. Devenish (2007), The U.K. Met Office's Next-Generation Atmospheric Dispersion Model, NAME III, in *Air Pollution Modeling and Its Application XVII*, edited by C. Borrego and A.-L. Norman, pp. 580–589, Springer, Boston, Mass.

Kai, F. M., S. C. Tyler, J. T. Randerson, and D. R. Blake (2011), Reduced methane growth rate explained by decreased Northern Hemisphere microbial sources, *Nature*, *476*(7359), 194–197, doi:10.1038/Nature10259.

Kao-Kniffin, J., D. S. Freyre, and T. C. Balser (2010), Methane dynamics across wetland plant species, *Aquat. Bot.*, *93*(2), 107–113, doi:10.1038/Nature10259.

Keeling, C. D. (1958), The concentration and isotopic abundances of atmospheric carbon dioxide in rural areas, *Geochim. Cosmochim. Acta*, *13*, 322–334.

Kirschke, S., et al. (2013), Three decades of global methane sources and sinks, *Nat. Geosci.*, *6*(10), 813–823, doi:10.1038/Ngeo1955.

Kort, E. A., et al. (2012), Atmospheric observations of Arctic Ocean methane emissions up to 82 degrees north, *Nat. Geosci.*, *5*(5), 318–321, doi:10.1038/Ngeo1452.

Kuhlmann, A. J., D. E. J. Worthy, N. B. A. Trivett, and I. Levin (1998), Methane emissions from a wetland region within the Hudson Bay Lowland: An atmospheric approach, *J. Geophys. Res.*, *103*, 16,009–16,016, doi:10.1029/98JD01024.

Laitenen, J., S. Rehell, A. Huttunen, T. Tahvanainen, R. Heikkilä, and T. Lindholm (2007), Mire systems in Finland—Special view to aapa mires and their water-flow pattern, *Suosera*, *58*(1), 1–26.

Levin, I., C. Veidt, B. H. Vaughn, G. Brailsford, T. Bromley, R. Heinz, D. Lowe, J. B. Miller, C. Poss, and J. W. C. White (2012), No inter-hemispheric delta(CH_4)-C-13 trend observed, *Nature*, *486*(7404), E3–E4, doi:10.1038/Nature11175.

Levy, P. E., et al. (2012), Methane emissions from soils: Synthesis and analysis of a large UK data set, *Global Change Biol.*, *18*(5), 1657–1669, doi:10.1111/j.1365-2486.2011.02616.x.

Lohila, A., et al. (2016), Large contribution of boreal upland forest soils to a catchment-scale CH_4 balance in a wet year, *Geophys. Res. Lett.*, *43*, 2946–2953, doi:10.1002/2016GL067718.

Lowry, D., C. W. Holmes, N. D. Rata, P. O'Brien, and E. G. Nisbet (2001), London methane emissions: Use of diurnal changes in concentration and $\delta^{13}C$ to identify urban sources and verify inventories, *J. Geophys. Res.*, *106*, 7427–7448, doi:10.1029/2000JD900601.

Lund Myhre, C., et al. (2016), Extensive release of methane from Arctic seabed west of Svalbard during summer 2014 does not influence the atmosphere, *Geophys. Res. Lett.*, *43*, 4624–4631, doi:10.1002/2016GL068999.

Marushchak, M. E., et al. (2016), Methane dynamics in the subarctic tundra: Combining stable isotope analyses, plot- and ecosystem-scale flux measurements, *Biogeosciences*, *13*(2), 597–608, doi:10.5194/bg-13-597-2016.

McCalley, C. K., et al. (2014), Methane dynamics regulated by microbial community response to permafrost thaw, *Nature*, *514*(7523), 478, doi:10.1038/nature13798.

Melton, J. R., et al. (2013), Present state of global wetland extent and wetland methane modelling: Conclusions from a model inter-comparison project (WETCHIMP), *Biogeosciences*, *10*(2), 753–788, doi:10.5194/bg-10-753-2013.

Mikaloff Fletcher, S. E., P. P. Tans, L. M. Bruhwiler, J. B. Miller, and M. Heimann (2004), CH_4 sources estimated from atmospheric observations of CH_4 and its C-13/C-12 isotopic ratios: 1. Inverse modeling of source processes, *Global Biogeochem. Cycles*, *18*, GB4004, doi:10.1029/2004GB002223.

Miller, S. M., et al. (2014), Observational constraints on the distribution, seasonality, and environmental predictors of North American boreal methane emissions, *Global Biogeochem. Cycles*, *28*, 146–160, doi:10.1002/2013GB004580.

Monteil, G., S. Houweling, E. J. Dlugokencky, G. Maenhout, B. H. Vaughn, J. W. C. White, and T. Rockmann (2011), Interpreting methane variations in the past two decades using measurements of CH_4 mixing ratio and isotopic composition, *Atmos. Chem. Phys.*, *11*(17), 9141–9153, doi:10.5194/acp-11-9141-2011.

Nisbet, E. G., and R. Weiss (2010), Top-down versus bottom-up, *Science*, *328*(5983), 1241–1243, doi:10.1126/science.1189936.

Nisbet, E. G., E. J. Dlugokencky, and P. Bousquet (2014), Methane on the rise-again, *Science*, *343*(6170), 493–495, doi:10.1126/science.1247828.

Olefeldt, D., M. R. Turetsky, P. M. Crill, and A. D. McGuire (2012), Environmental and physical controls on northern terrestrial methane emissions across permafrost zones, *Global Change Biol.*, *19*(2), 589–603, doi:10.1111/gcb.12071.

Öquist, M. G., and B. H. Svensson (2002), Vascular plants as regulators of methane emissions from a subarctic mire ecosystem, *J. Geophys. Res.*, *107*(D21), 4580, doi: 10.1029/2001JD001030.

O'Shea, S. J., S. J. B. Bauguitte, M. W. Gallagher, D. Lowry, and C. J. Percival (2013), Development of a cavity-enhanced absorption spectrometer for airborne measurements of CH_4 and CO_2, *Atmos. Meas. Tech.*, *6*(5), 1095–1109, doi:10.5194/amt-6-1095-2013.

O'Shea, S. J., et al. (2014), Methane and carbon dioxide fluxes and their regional scalability for the European Arctic wetlands during the MAMM project in summer 2012, *Atmos. Chem. Phys.*, *14*(23), 13,159–13,174, doi:10.5194/acp-14-13159-2014.

Pataki, D. E., J. R. Ehleringer, L. B. Flanagan, D. Yakir, D. R. Bowling, C. J. Still, N. Buchmann, J. O. Kaplan and J. A. Berry (2003), The application and interpretation of Keeling plots in terrestrial carbon cycle research, *Global Biogeochem. Cycles*, *17*(1), 1022, doi:10.1029/2001GB001850.

Petrescu, A. M. R., L. P. H. van Beek, J. van Huissteden, C. Prigent, T. Sachs, C. A. R. Corradi, F. J. W. Parmentier, and A. J. Dolman (2010), Modeling regional to global CH₄ emissions of boreal and arctic wetlands, *Global Biogeochem. Cycles*, *24*, GB4009, doi:10.1029/2009GB003610.

Pickett-Heaps, C. A., D. J. Jacob, K. J. Wecht, E. A. Kort, S. C. Wofsy, G. S. Diskin, D. E. J. Worthy, J. O. Kaplan, I. Bey, and J. Drevet (2011), Magnitude and seasonality of wetland methane emissions from the Hudson Bay Lowlands (Canada), *Atmos. Chem. Phys.*, *11*(8), 3773–3779, doi:10.5194/acp-11-3773-2011.

Poindexter, C. M., D. D. Baldocchi, J. H. Matthes, S. H. Knox, and E. A. Variano (2016), The contribution of an overlooked transport process to a wetland's methane emissions, *Geophys. Res. Lett.*, *43*, 6276–6284, doi:10.1002/2016GL068782.

Portnov, A., A. J. Smith, J. Mienert, G. Cherkashov, P. Rekant, P. Semenov, P. Serov, and B. Vanshtein (2013), Offshore permafrost decay and massive seabed methane escape in water depths > 20 m at the south Kara Sea shelf, *Geophys. Res. Lett.*, *40*, 3962–3967, doi:10.1002/Grl.50735.

Rice, A. L., S. C. Tyler, M. C. McCarthy, K. A. Boering, and E. Atlas (2003), Carbon and hydrogen isotopic compositions of stratospheric methane: 1. High-precision observations from the NASA ER-2 aircraft, *J. Geophys. Res.*, *108*(D15), 4460, doi:10.1029/2002JD003042.

Röckmann, T., M. Brass, R. Borchers, and A. Engel (2011), The isotopic composition of methane in the stratosphere: High-altitude balloon sample measurements, *Atmos. Chem. Phys.*, *11*(24), 13,287–13,304, doi:10.5194/acp-11-13287-2011.

Santoni, G. W., B. H. Lee, J. P. Goodrich, R. K. Varner, P. M. Crill, J. B. McManus, D. D. Nelson, M. S. Zahniser, and S. C. Wofsy (2012), Mass fluxes and isofluxes of methane (CH₄) at a New Hampshire fen measured by a continuous wave quantum cascade laser spectrometer, *J. Geophys. Res.*, *117*, D10301, doi:10.1029/2011JD016960.

Saunois, M., et al. (2016), The global methane budget 2000–2012, *Earth Syst. Sci. Data*, *8*, 697–751, doi:10.5194/essd-8-697-2016.

Schaefer, H., et al. (2016), A 21st century shift from fossil-fuel to biogenic methane emissions indicated by ¹³CH₄, *Science*, doi:10.1126/science.aad2705.

Schwietzke, S., et al. (2016), Upward revision of global fossil fuel methane emissions based on isotope database, *Nature*, doi:10.1038/nature19797.

Shakhova, N., et al. (2014), Ebullition and storm-induced methane release from the East Siberian Arctic Shelf, *Nat. Geosci.*, *7*(1), 64–70, doi:10.1038/Ngeo2007.

Sriskantharajah, S., R. E. Fisher, D. Lowry, T. Aalto, J. Hatakka, M. Aurela, T. Laurila, A. Lohila, E. Kuitunen, and E. G. Nisbet (2012), Stable carbon isotope signatures of methane from a Finnish subarctic wetland, *Tellus Ser. B*, *64*, doi:10.3402/Tellusb.V64i0.18818.

Strom, L., A. Ekberg, M. Mastepanov, and T. R. Christensen (2003), The effect of vascular plants on carbon turnover and methane emissions from a tundra wetland, *Global Change Biol.*, *9*(8), 1185–1192, doi:10.1046/j.1365-2486.2003.00655.x.

Sugawara, S., T. Nakazawa, Y. Shirakawa, K. Kawamura, S. Aoki, T. Machida, and H. Honda (1997), Vertical profile of the carbon isotopic ratio of stratospheric methane over Japan, *Geophys. Res. Lett.*, *24*, 2989–2992, doi:10.1029/97GL03044.

Thornton, B. F., M. Wik, and P. M. Crill (2015), Climate-forced changes in available energy and methane bubbling from subarctic lakes, *Geophys. Res. Lett.*, *42*, 1936–1942, doi:10.1002/2015GL063189.

Tsuruta, A., et al. (2016), Development of CarbonTracker Europe-CH4—Part 2: Global methane emission estimates and their evaluation for 2000–2012, *Geosci. Model Dev. Discuss.*, doi:10.5194/gmd-2016-182.

Umezawa, T., T. Machida, S. Aoki, and T. Nakazawa (2012), Contributions of natural and anthropogenic sources to atmospheric methane variations over western Siberia estimated from its carbon and hydrogen isotopes, *Global Biogeochem. Cycles*, *26*, GB4009, doi:10.1029/2011GB004232.

Walter, K. M., J. P. Chanton, F. S. Chapin, E. A. G. Schuur, and S. A. Zimov (2008), Methane production and bubble emissions from arctic lakes: Isotopic implications for source pathways and ages, *J. Geophys. Res.*, *113*, G00A08, doi:10.1029/2007JG000569.

Warwick, N. J., M. L. Cain, R. Fisher, J. L. France, D. Lowry, S. E. Michel, E. G. Nisbet, B. H. Vaughn, J. W. C. White, and J. A. Pyle (2016), Using δ¹³C-CH₄ and δD-CH₄ to constrain Arctic methane emissions, *Atmos. Chem. Phys.*, *16*, 14,891–14,908, doi:10.5194/acp-16-14891-2016.

Westbrook, G. K., et al. (2009), Escape of methane gas from the seabed along the West Spitsbergen continental margin, *Geophys. Res. Lett.*, *36*, L15608, doi:10.1029/2009GL039191.

Whiticar, M. J., E. Faber, and M. Schoell (1986), Biogenic methane formation in marine and fresh-water environments—CO₂ reduction vs acetate fermentation isotope evidence, *Geochim. Cosmochim. Acta*, *50*(5), 693–709, doi:10.1016/0016-7037(86)90346-7.

Wik, M., P. M. Crill, R. K. Varner, and D. Bastviken (2013), Multiyear measurements of ebullitive methane flux from three subarctic lakes, *J. Geophys. Res. Biogeosci.*, *118*, 1307–1321, doi:10.1002/jgrg.20103.

WMO (2015), WMO Greenhouse Gas Bulletin (11).

Worthy, D. E. J., I. Levin, F. Hopper, M. K. Ernst, and N. B. A. Trivett (2000), Evidence for a link between climate and northern wetland methane emissions, *J. Geophys. Res.*, *105*, 4031–4038, doi:10.1029/1999JD901100.

Yvon-Durocher, G., A. P. Allen, D. Bastviken, R. Conrad, C. Gudasz, A. St-Pierre, N. Thanh-Duc, and P. A. del Giorgio (2014), Methane fluxes show consistent temperature dependence across microbial to ecosystem scales, *Nature*, *507*(7493), 488–491, doi:10.1038/Nature13164.

Zazzeri, G., D. Lowry, R. E. Fisher, J. L. France, M. Lanoisellé, and E. G. Nisbet (2015), Plume mapping and isotopic characterisation of anthropogenic methane sources, *Atmos. Environ.*, *110*, 151–162, doi:10.1016/j.atmosenv.2015.03.029.

Zazzeri, G., et al. (2016), Carbon isotopic signature of coal-derived methane missions to the atmosphere: From coalification to alteration, *Atmos. Chem. Phys.*, *16*, 13,669–13,680, doi:10.5194/acp-16-13669-2016.